Zivkovic V, Ridge N, Biggs MJ.

Experimental study of efficient mixing in a micro-fluidized bed.

***Applied Thermal Engineering* (2017)**

DOI: https://doi.org/10.1016/j.applthermaleng.2017.08.144

Experimental study of efficient mixing in a micro-fluidized bed

Vladimir Zivkovic[1*], Nadia Ridge[2], Mark J. Biggs[2,3]

*Corresponding author: Tel.: +44 (0)191 2084865; Fax: +44 (0) 191 208 5292; Email: vladimir.zivkovic@ncl.ac.uk
1 School of Engineering, Newcastle University, Newcastle, NE1 7RU, UK
2 School of Chemical Engineering, The University of Adelaide, Adelaide, 5005, Australia
3 School of Science, Loughborough University, Loughborough, LE11 3TU, UK

Abstract

Micro-fluidized beds represent a novel means of significantly enhancing mixing and mass and heat transfer under the low Reynolds number flows that dominate in microfluidic devices. This study experimentally evaluates the mixing performance of a micro-fluidized bed and the improvements it affords over the equivalent particle-free system. The dye dilution technique coupled with standard top-view image analysis was used to characterize the mixing in a 400 x 175 μm^2 polydimethylsiloxane (PDMS) Y-microchannel. Overall, the micro-fluidized bed provided a mixing effectiveness and energetic efficiency of mixing that were up to three times greater than those of a particle-free channel of the same dimensions. The mixing performance is strongly affected by specific power input and bed voidage. The optimal operating voidage, which corresponds to the energetic efficiency of mixing being maximal, is around 0.77 for the smallest particle-to-channel size ratio considered here 0.121, and appears to increase beyond this with size ratio.

Keywords: Fluidization; Mixing efficiency; Micro-fluidized bed; Micro-mixer; Multiphase flow; Process intensification.

1. Introduction

Chemical micro-process technologies are a relatively new concept that offers much promise in terms of achieving process intensification [1]. In the context of micro-process technologies the most important units are micro-reactors that take advantage of excellent mass and heat transfer characteristics of micro-structured devices [1, 2]. Such micro-reactors have already found application in industrial plants in so-called 'scaled-out' systems that are capable of production rates greater than their conventional counterparts in far smaller volumes [1]. Another very important application of micro-devices is in the high-heat flux cooling of computer micro-chips and datacentres [3, 4], and in compact heat exchangers in the refrigeration, power, automotive, chemical, cryogenics and aerospace sectors [5-7]. A closely related field that is arguably the precursor of chemical micro-processing is microfluidics [8-11]. The main aim of microfluidics [12, 13] is to scale down and integrate laboratory functions in a miniaturized chip format termed lab-on-a-chip [14]. Some applications of these microfluidic devices include point-of-care diagnostics [15, 16], cell biology and biochemical analysis [17], high-throughput screening in drug discovery [18], genomics [19] and proteomics [20].

Mixing phenomena are often core to chemical processing, particularly those that involve heat transfer, mass transfer and reaction. One challenge for chemical micro-processes in such circumstances is the almost universality of laminar flow that limits heat and mass transport rates to

that of molecular diffusion. Many micro-mixer technologies have been developed to overcome this 'slow' molecular diffusion limit in suitable time and length scales [21, 22]. In general, micromixers can be classified as either active or passive depending on whether or not they employ an external energy source to promote mixing, in addition to that driving the flow through the device [23-25]. Ultimately, all proposed micro-mixing methods lead to increase in the pressure drop (energy consumption), so one should take both mixing quality and energy consumption into consideration when selecting a micro-mixer. It is for this reason that Kockmann *et al.* [26] introduced the mixing effectiveness factor, which takes into account both mixing quality and the pressure drop to evaluate micro-mixers. An alternative to this introduced by Falk and Commenge [27] is the energetic efficiency of mixing, which is based on specific power consumption.

The micro-fluidized bed (μFB) [28, 29], which is essentially fluidization of micron-sized particles in channels of sub-centimetre cross-section, can provide enhancement of mixing, mass and heat transfer for micro-devices due to the chaotic motion of the fluidized particles [30-32]. Since its initial introduction by Potic *et al.* [33], only a small number of studies have been reported on liquid fluidization in μFB. Whilst some of these studies have been application-focused [34, 35], the vast majority have focused on hydrodynamic aspects of μFBs [28, 31, 36, 37] and the effects of surface forces and wall effects on their fluidization behaviour [28, 29, 38, 39]. Of these, only Doroodchi *et al.* [31] have focused in detail on mixing. In their study, fluidization of a bed of ~98 μm diameter borosilicate particles by a sodium iodide flow in a 1.2 mm diameter capillary of the same material was shown to reduce the mixing time to less than an eighth of that in the absence of particles. Although this study shows μFBs have the potential to substantially improve mixing, it was limited in scope as only three different liquid flow rates were considered; the relationship between bed voidage and mixing performance was not elucidated at all even though it is known that this relationship is important in macroscopic counterparts [40].

The study reported here is an experimental investigation into the mixing performance of a μFB. Trials were carried out on a bed of glass micron-sized spheres (~30, 35 and 40 μm in diameter) fluidized by a flow of ethanol in a 400 x 175 μm^2 polydimethylsiloxane (PDMS) Y-channel. The mixing was determined using standard top-view imaging techniques along the micro-channel length of dyed and transparent sample streams as they mix in the channel. The performance in mixing that this μFB is capable of delivering compared to the same system without particles is quantified; the mixing effectiveness factor [26] and energetic efficiency of mixing [27] were both used to study the mixing performance and the trade-off between this and the energy input required. This study constitutes the first to evaluate the mixing performance of a μFB whose cross-section is sub-mm in size as a function of different flow rates and corresponding bed voidages, and particle-to-channel size ratio.

2. Experimental Details and Methodology

2.1. The Micro-Fluidized Bed

The experimental set-up is shown in Figure 1. The μFB, which is schematically shown in Figure 1(a), was fixed vertically in a holder custom made for the micro-bed chips and mounted on a height-adjustable rotary stage (M488, Newport Corporation, USA). The stage allowed ready study of regions along the length of the μFB. A multi-feed syringe pump (PHD ULTRA, Harvard Apparatus, US) introduced the fluidizing medium at the desired flow rates through the two input ports of the Y-

channel (see below for further detail on this). Digital movies of the flow in the μFB were recorded at a rate of 25 frames/s using a CCD camera (KY-F550E, JVC, Japan) coupled to a trinocular stereomicroscope with fibre optic illuminator (SMZ-168-TH, Motic, China) and stored on a PC for offline analysis.

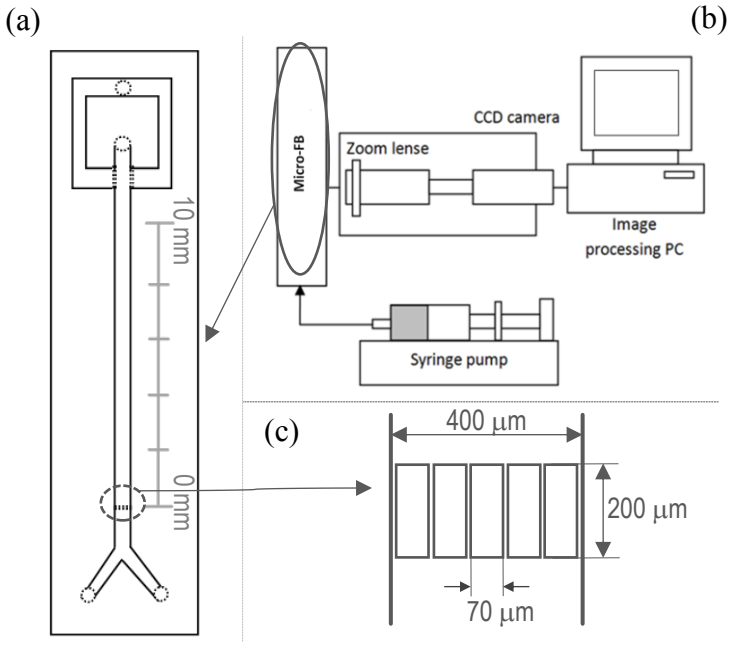

Figure 1. Schematics of experimental set-up: (a) close-up schematics of the μFB chip; (b) the top-view flow visualisation along the micro-channel length; and (c) close-up schematic of the pillar-based distributor of the μFB.

The microchannel hosting the fluidized bed was formed in polydimethylsiloxane (PDMS) using standard soft lithography techniques [41]. The microchannel was 10 mm long and had a rectangular cross-section of 400 μm by 175 μm. A ruler etched onto the platform beside the microchannel facilitated easy bed height tracking and measurement. The fluidized bed distributor, Figure 1(c), designed using computational fluid dynamics [42], comprised of a series of five 70 μm wide and 200 μm long rectangular pillars separated by 8-9 μm gaps. Experiments were performed at an ambient temperature of 25 ± 1°C.

2.2. Fluidizing Material

The bed particles were as-supplied glass microspheres (CoSpheric LLC, CA, USA) of density 2500 kg/m^3. Particles of three narrowly-distributed sizes were considered: average diameters of d_p = 29.5, 34.5 and 39.5 μm with a standard deviation of 1.5 μm. Particles were loaded into the channel through the outlet as an anhydrous ethanol (≥99.5% from Sigma Aldrich, St. Louis, MO) based slurry that was allowed to settle under gravity to form a packed bed. The same ethanol was also used to fluidise the particles.

The scale of microfluidized beds means surface forces can be comparable to the hydrodynamic forces. This makes particle aggregation and adhesion to the bed wall a potential issue, even to the point of preventing fluidization [28, 29]. The acid-base model of van Oss, Chaudhury and Good combined with the Derjaguin approximation can be used to predict wall material/particle/fluid triplets that avoid this issue [29, 38, 39]. In the case of the wall material/particle pair considered

here, we have both predicted and demonstrated [29] that ethanol is a suitable fluidizing medium, hence why it has been used in the work reported here.

In order to elucidate mixing in the μFB, ethanol coloured with a commercial blue dye (E133, Queen Fine Foods Pty Ltd, Australia) was injected into one of the ports of the Y-channel whilst uncoloured ethanol was injected through the other at the same rate (*i.e.* the total flow rate was split evenly between the two channels). The total inlet flow rate was decremented from 1600 nL/min to 200 nL/min in 200 nl/min steps every minute. As steady bed behaviour was achieved about 30 s after the step change, the last 30 seconds at a given flow rate were the focus of the subsequent analysis. The decreasing of the flow rate here averts pressure overshoot, which may be present due to the large particle-to-bed size ratios of the system (d_p/D_h ~ 0.12 to 0.16 based on the micro-channel hydraulic diameter, D_h ~ 243.5μm, see Table 1) [36]. As a baseline for comparison of mixing behaviour, identical trials were also carried out in the same channel with no particles present. Two independent runs were performed for each mixing study with or without particles.

2.3. Bed Fluidization Characteristics

The bed voidage, ε, was calculated by [28, 40].

$$\varepsilon = 1 - \left(1 - \varepsilon_{mf}\right)\frac{h_0}{h} \quad (2)$$

where ε_{mf} is the minimum fluidization voidage and h_o and h are the initial (static) and steady-state operating bed heights. The static bed height was measured under zero inlet flow at the beginning of each experiment. A series of 100 steady-state height measurements were recorded from image stacks at any given flow rate and the final h value taken as the average of these. Values of ε_{mf} as shown in Table 1 were estimated by interpolation from prior work of the authors [43, 44]. To account for interpolation error and for the difference between the micro-channel and capillary (aspect ratio and material), the absolute error accompanying voidage estimates was doubled.

The expansion behaviour of the μFB was well described by the Richardson-Zaki correlation [45]

$$U = kU_t\varepsilon^n \quad (3)$$

where U and U_t are superficial velocity and the particle settling velocity respectively, k an empirical parameter, and n the Richardson-Zaki exponent. The value of the latter is also provided in Table 1.

Table 1. Characteristics of bed properties for the different micro-particles studied in the micro-fluidized bed.

Average particle size d_p (μm)	Particle-to-bed size ratio, d_p/D_h	Initial bed height h_o (mm)	Estimated packed bed voidage, ε_{mf}	Richardson-Zaki exponent, n
29.5	0.121	2.0	0.49 ± 0.03	5.4 ± 0.4
34.5	0.142	2.2	0.52 ± 0.03	6.1 ± 0.6
39.5	0.162	2.6	0.55 ± 0.03	7.4 ± 0.8

2.4. Mixing performance

The basis for assessing the mixing performance was the uniformity of the dye distribution in rectangular regions of interest (ROIs) in the freeboard of the μFB (see Figure 2) or the micro-channel when operating under steady-state conditions. This was determined from analysis of the digital movies captured by the CCD camera. This analysis involved multiple steps. The first was splitting the movies into stacks of images using the VirtualDub software. Each of the images in the stack were then analysed using the ImageJ software [46]. This first involved splitting the images into the

RGB channels. The red (R) channel images were then subject to statistical analyses to determine the effectiveness of mixing in terms of the *relative mixing index* [47, 48]

$$\eta = \frac{\sigma_o - \sigma}{\sigma_o - \sigma_\infty} \qquad (1)$$

where σ is the standard deviation of pixel intensity values within the ROI, and the subscripts 'o' and '∞' denote the initial unmixed and final completely mixed states of the fluid streams. Values for σ_o and σ_∞ were obtained in the particle-free channel operated zero inlet and at the maximum flow rates, respectively. This relative form of the mixing index was used as it is very robust due to insensitivity to variation in light intensities as well as to the colour of the dye used [48].

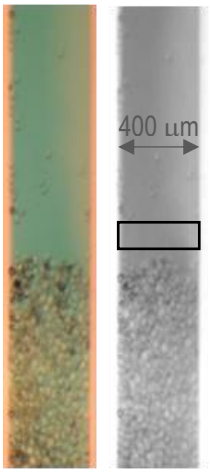

Figure 2. (colour online) Colour RGB image of the micro-fluidized bed as captured by the camera (left) and corresponding grey scale image obtained from a single (red) channel of the RGB original image (right). The region that is subject to image analysis to determine the degree of mixing (the region of interest or ROI) is indicated by the rectangle in the right-hand image.

The relative mixing index was used as a basis for evaluating two different measures of mixing performance that account for the energy input. The first of these measures was the *mixing effectiveness factor* of Kockmann *et al.* [26], which is given by

$$ME_I = \frac{D_h \rho U^2}{l_m \Delta p} \qquad (4)$$

where ρ is the fluid density, l_m the mixing length [26], and Δp the pressure drop across the bed/channel length. The pressure drop of the channel without any particles present was calculated using the analytical expression for Poiseuille flow [49], while the pressure drop across the fluidized bed was equated to the buoyant weight of the bed particles [36]. The mixing length was determined from the plots of the relative mixing index as a function of the distance from the channel inlet by linear extrapolation for the empty channel and exponential fitting for the fluidized bed [31].

The second measure for quantifying mixing performance is the *energetic efficiency of mixing* of Falk and Commenge [27], which is given by ratio of shear rates following Ottino *et al.* [50]

$$\eta = \frac{\gamma}{\gamma_{max}} \qquad (5)$$

where γ is shear rate used effectively for mixing, and γ_{max} is total shear rate. The latter can be evaluated using

$$\gamma_{max} = \left(\frac{\varepsilon_e \rho}{2\mu}\right)^2 \qquad (6)$$

where μ is fluid viscosity, and ε_e is specific power dissipation rate. The specific energy dissipation rate is given by

$$\varepsilon_e = \frac{Q\Delta p}{\rho V} \tag{7}$$

where Q is the volumetric flow rate, and V is the volume of the mixer. The effective shear rate γ is obtained by fitting the mixing time to the theoretical expression of Baldyga and Bourne [51] on mixing by diffusion in a shear flow given by

$$t_{mix,t} = \frac{\operatorname{arcsinh}\left(\frac{0.76\gamma\delta^2}{D}\right)}{2\dot{\gamma}} \tag{8}$$

where δ is the thickness of striation, which is half of channel width in our case, D is diffusion coefficient, and the mixing time is obtained using [26]

$$t_m = \frac{l_m}{U} \tag{9}$$

3. Results and Discussion

3.1. Fluidization Behaviour of the Micro-Fluidized Bed

Figure 3 shows images of the bed expansion at steady state under different inlet volumetric flow rates. The overall behaviour of the bed matched that described in our previous reports [28, 29]. As predicted [29], ethanol proved to be a good fluidising medium for the glass particle/PDMS microchannel system used here, with smooth and stable homogenous fluidization. A slightly asymmetric distribution of flow was evident in the distributor region, which caused some flow channelling on the right-hand side of the beds. Minor blockages of central distributor apertures with particles are thought to be the cause of this. Very minimal adhesion of particles to the channel walls occurred, which is similar to observations of our previous experimental work [29]. A distinct interface between the top of the bed of particles and freeboard above it was observed for all flow rates, although it became increasingly less-well defined for flow rates above 1200 nL/min.

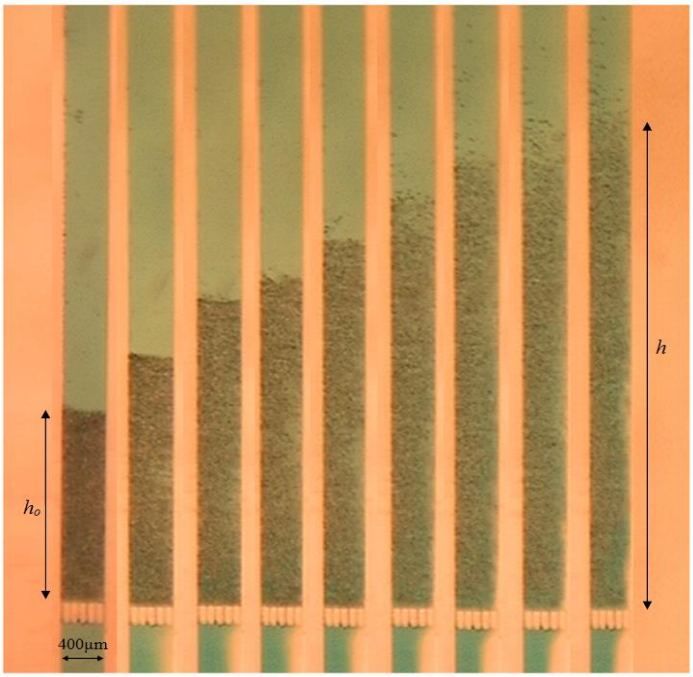

Figure 3. (colour online) Images of the micro-fluidized bed of 29.5 µm glass particles at different flow rates. The first image on far left is of packed bed (no flow) while others show micro-fluidized bed with flow rates increasing in 200 nL/min increments from 200 nL/min to 1600 nL/min (left to right). The initial bed height h_o and fluidized bed height h are indicated.

Experimentally determined minimum fluidization velocities were well-predicted by the Ergun equation [52] provided the enhancement in bed porosities due to wall effects (see Table 1) are used. This supports the idea that the classical fluidization models are still valid for the analysis and design of μFBs, in line with previous studies [28, 29, 36].

In the original work of Richardson and Zaki [45], the exponent n was correlated by a five-part empirical equation as a function of the Reynolds number, Re, and the particle-to-bed size ratio, d_p/D_h, which captures wall effects. The prediction of the exponent from these equations for the Stokes regime (Re < 0.2) in the absence of wall effects is 4.65 [45]. As the exponents determined here, which are shown in Table 1, are greater than this and increase with the particle-to-bed ratio, it appears that wall effects are significant for the systems studied here. This is in line with our previous study [39], albeit the values here are approximately 10-15% higher. This may be due to difference in the wall material as square glass capillary were utilized in our previous study. In contrast, Tang *et al.* [37] determined slightly lower values of the exponent n than the correlation predictions but, as suggested by these authors, the likely reason is a wide particle size distribution that is not present here.

The Richardson and Zaki constants k is around 2 for all systems studied here. This is in line with our initial study [28] as well as that of Tang *et al.* [37], but contrasts with our earlier micro-fluidization experiments in glass micro-capillaries [39], which were more in line with macroscopic experiments where the k values were around 0.75. Once again this difference is probably due to different bed materials as Tang *et al.* also used polymeric (PMMA) fluidized beds.

3.2. Mixing Index and Length

Figure 4 shows a comparison between typical images of mixing in the micro-fluidized bed and in the particle-free baseline at three different operating fluid volumetric flow rates and corresponding superficial velocities (volumetric flowrate divided by cross section area). Improvement in the degree of mixing for the micro-fluidized bed in comparison with the particle free channel is visually evident for all the flow rates. In order to establish the flow rate that maximises the degree of mixing, we analysed the images as described in the method section to determine the relative mixing index from Equation (1).

Figure 5(a) shows the relative mixing index for a particle-free channel as a function of distance above the distributor at four different superficial velocities (trends are similar for all other studied flow rates). The clear linear trend seen here (coefficient of determination $R^2 > 0.995$ in all cases) greatly facilitates the evaluation of mixing index of the ROIs in the various μFBs relative to the same distance from the distributor for the empty channel; this is important for direct comparison between the performance of the empty micro-channel the micro-fluidized beds (this is exploited in Figure 6(a)). Somewhat surprisingly, the linear fits in Figure 5(a) do not pass through the origin. This is, however, in line with previous studies by others [31, 53].

The mixing length for the particle-free channel, which is obtained by extrapolating the mixing index lines in Figure 5(a) to $\eta = 1$, are in the range of 10 to 18 mm which is similar to that reported by Hsieh *et al.* [53], who studied a channel of similar size to that considered here (200 by 200 μm cross section). Figure 5(b) indicates the mixing length increases in a linear manner with superficial velocity (coefficient of determination R^2 is 0.98). This is as expected for a fixed channel size and fluid as the mixing length for flows in molecular diffusion dominates is known to increase with Reynolds Number [24].

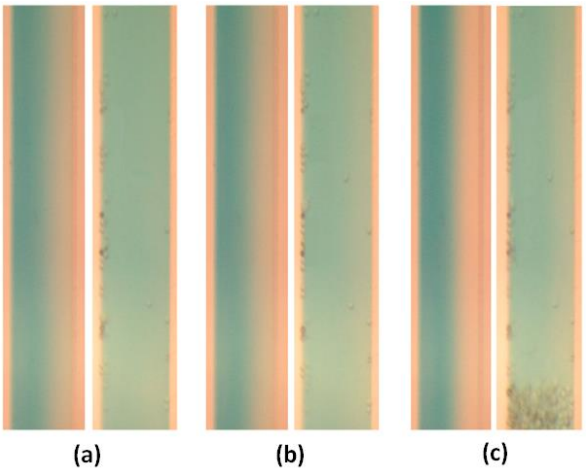

Figure 4. Comparison between mixing in the particle-free channel (leftmost image in each of the three plate sets) and in the particle free zone above the micro-fluidized bed (rightmost image in each of the three plate sets) composed of 29.5 μm glass particles at three different fluid flow rates (corresponding superficial velocities, *U*, are given here in the parentheses): (a) 800 nL/min (190 μm/s); (b) 1200 nL/min (286 μm/s); and (c) 1600 nL/min (361 μm/s).

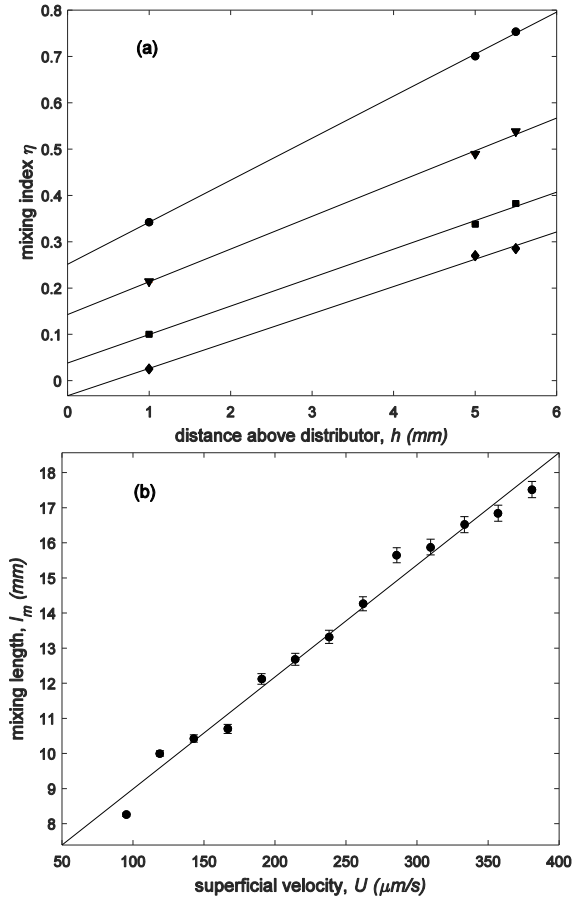

Figure 5. (a) Variation of the average mixing index in a particle-free channel as a function of distance above the distributor for superficial velocities of 95 μm/s (circles), 190 μm/s (triangles), 286 μm/s (squares) and 381 μm/s (diamonds); and (b) variation of mixing length, l_m, determined from extrapolation of data in (a) with the fluid velocities. Lines are linear fitting of experimental points. E*rror bars* are the standard errors of for the average and a predicted value. An absence of *error bars* means the errors are smaller than the size of the symbol.

Figure 6(a) shows the variation of mixing index with inlet velocity for both a micro-fluidized bed of 29.5 μm glass particles and for the particle-free channel at a distance from the distributor that is

equal to that of the ROI of the FB. The mixing index for the channel decreases from around 0.5 at a superficial velocity of 100 μm/s to around 0.3 at 350 μm/s, with the rate of decrease diminishing mildly due to its dependence on the superficial velocity and change in the distance from the distributor due to it being equal to that of the ROI in the fluidized bed. In contrast, the mixing index of the μFB varies very little with superficial velocity: it first increases from 0.97 at the lowest superficial velocity of 95 μm/s to a maximum of nearly 0.99 at the fluid velocity of 190 μm/s (this corresponds to Figure 4(a)), before dropping off again weakly as the fluid velocity increases to 0.90 for the highest velocities considered here. The trends are very similar for other two particles sizes studied here. This very simplified analysis would suggest the best operating point of the μFB mixer to be at intermediate inlet fluid velocity and flowrate.

The improvement in mixing provided by the micro-fluidized bed over the particle-free channel can be clearly understood by taking the ratio of the mixing indexes of the two as shown in Figure 6(b). This figure indicates that, depending on the superficial velocity, the μFB improves mixing by between 2 and 3 times that of a straight channel of the same length. Interestingly, there appears to be an upper limit to the improvement with flow rate, which is elucidated further in the next section.

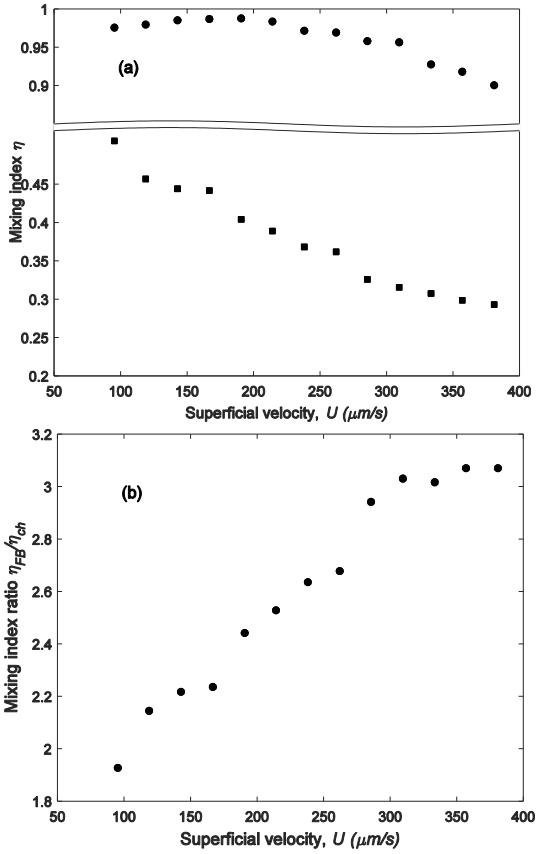

Figure 6. (a) The variation of mixing index for micro-fluidized bed η_{FB} (circles) with 29.5 μm particles and corresponding mixing index in particle-free channel η_{ch} (squares) at the same bed height, h (i.e. distance from the distributor)*;* and (b) ratio of the mixing index of the μFB to that of the channel alone as a function of the inlet fluid velocity, U. Absence of *error bars* indicates the standard errors of the mean (a) and a predicted value (b) are no greater than the size of the symbol.

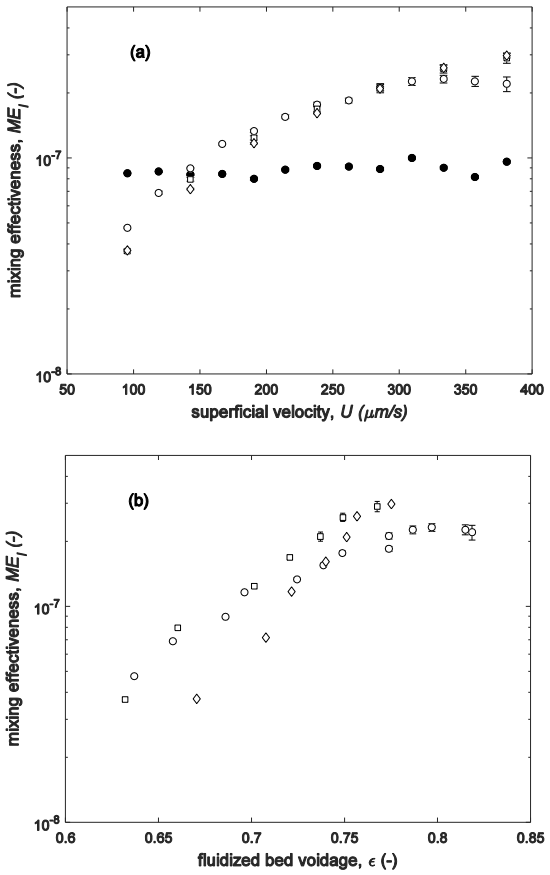

Figure 7. The mixing effectiveness factor [26] of particle-free channel (filled circles) and micro-fluidized beds of 29.5 μm (open circles), 34.5 μm (open squares) and 39.5 μm (open diamonds) glass micro-particles as a function of: (a) superficial fluid velocity; and (b) fluidized bed voidage. Error bars are standard errors of calculated values. An absence of error bars means the errors are smaller than the size of the symbol.

3.3. Mixing Effectiveness

The relative mixing index of the previous section does not account for the trade-off between increased mixing and the energy input required to achieve this. The mixing effectiveness (ME) defined in Eq. (4) is one way of evaluating this trade-off. This quantity is shown in Figure 7(a) for the particle-free channel and μFB as a function of the inlet fluid velocity. The ME of the particle-free channel appears to be little affected by superficial velocity, consistent with both our previous studies [26, 54] and the fact that transport will be essentially controlled by molecular diffusion. The μFB results indicate that it is not as effective as the particle-free channel at superficial velocities below around 150 μm/s. At higher velocities, the μFB can provide up to 2.8 times improvements in the mixing performance slightly lower than 3.1 times direct increase in mixing quality, suggesting that the energy consumption penalty for mixing improvement is relatively low. For all micro-fluidized beds, the effectiveness increases steadily with the superficial velocity except for the fluidization of 29.5 μm particles, which plateaus for velocities above 330 μm/s.

The observed plateau for the 29.5 μm particles can be understood by considering the mixing effectiveness as a function of the bed voidage as shown in Figure 7(b). In the case of these particles, the maximum in mixing effectiveness factor is achieved at a bed voidage of around 0.78. This is in agreement with the simple empirical prediction, $\varepsilon_{max}= (n\text{-}1)/n$ proposed for macroscopic fluidized

beds [40], which predicts a voidage of 0.81 based on the Richardson-Zaki exponent of n = 5.4 (see Table 1). Similarly, Yang *et al.* [34] observed the best performance of mini-FB photocatalytic reactor at a bed voidage of 0.75, once again broadly consistent with this simple empirical prediction as $n \approx 5$ in their study. Using the exponents reported in the Table 1 for the two larger particle sizes of 34.5 and 39.5 μm, the maximum mixing effectiveness factor should occur at voidages of 0.83 and 0.86 respectively. As these voidages were not probed in the study here, the maxima for these larger particles will not be seen in Figure 7(a), nor the accompanying plateau in Figure 7(b).

3.4. Energetic Efficiency of Mixing

The energetic efficiency of mixing (η), which is defined in Eq. (5), is an alternative way of quantifying the trade-off between mixing performance and the energy input. This quantity is shown in Figure 8(a) for the empty channel and three μFBs as a function of the specific power dissipation. For the micro-channel, after an initial plateau of 1.6% at low dissipation rates (*i.e.* flow rates), the efficiency of mixing decreases with increasing dissipation rate to around 1.1% at the highest dissipation rates encountered for the channel (*i.e.* around 0.008 W/kg). This drop off is entirely consistent with the molecular diffusion limit that prevails in the micro-channel, which is clearly unaffected by flow rate that requires additional power to increase.

Inspection of Figure 8(a) shows that the energetic efficiency of mixing in the μFB at the lowest dissipation rates encountered here (*i.e.* flow rates considered here) is less than the upper limit for the micro-channel. Beyond this, however, the energetic efficiency of mixing for the μFBs quickly takes off with increasing power dissipation (*i.e.* flow rate). This behaviour relative to that of micro-channel is entirely consistent with Figure 7(a), including the cross-over in mixing effectiveness of the two configurations at the lower end of the fluid velocity (*i.e.* power dissipation) range.

The behaviour seen in Figure 8(a) confirms that mixing performance of microfluidized beds are strongly dependent on the specific power input. This figure is also suggestive that this link is a direct one. However, the last few of points for the smallest particle size considered here, which are indicated by the arrows in the figure, are clearly at variance with this idea. This behaviour arises from the fact that the optimal mixing point for this particle size has been passed at these higher power dissipations, as discussed above and better seen in Figure 8(b). Whilst a maximum is not observed directly for the other two particle sizes, the energetic efficiency variation with voidage in Figure 8(b) appears to plateau at the upper end of voidage range considered, suggesting a maximum is located not far above the range investigated. This is consistent with the analysis of Figure 7(b) and the associated Richardson-Zaki based analysis presented at the end of the previous section.

Figure 8 shows that only about 2-3 percent of the total power input to the μFBs is effectively used for mixing, similar to other types of complex micro-mixer [27] and, indeed, in the only other prior study on mixing in μFBs [31]. However, comparison with empty channel shows that this transfer of energy into mixing is up to 2.6 times higher than that achieved by the channel alone for the same specific power consumption.

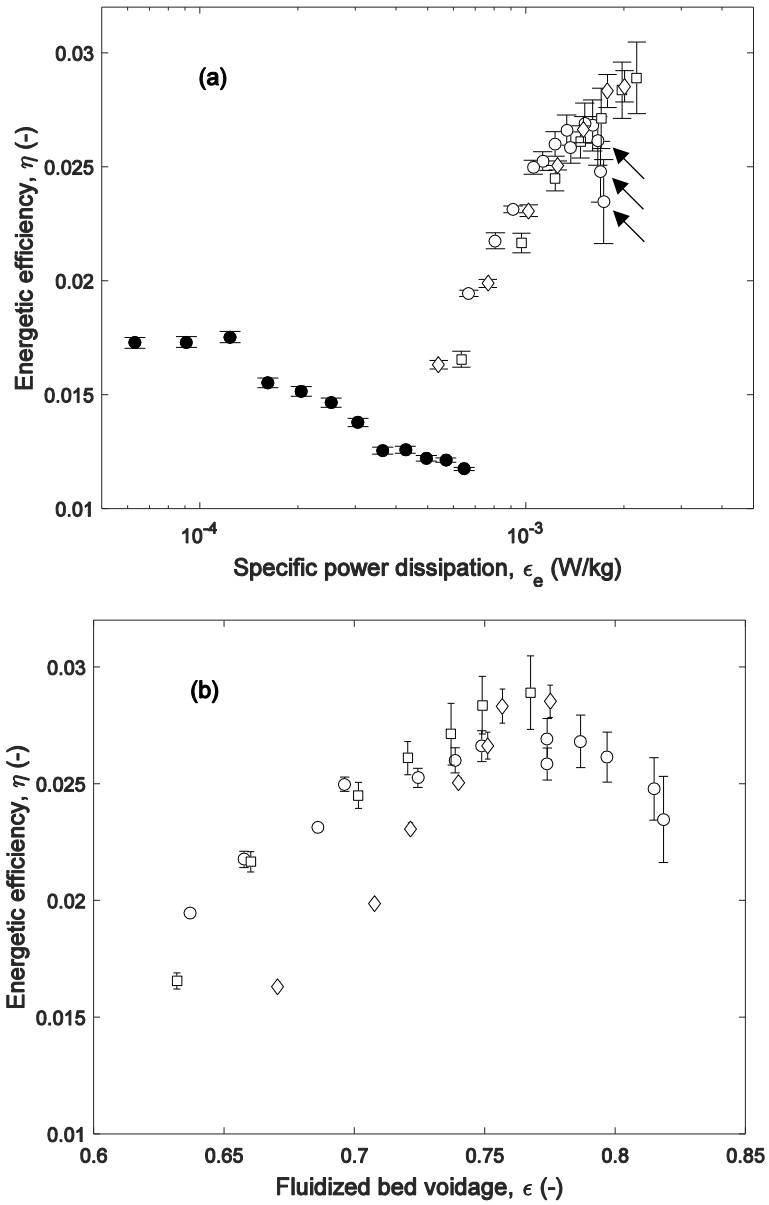

Figure 8. The energetic efficiency of mixing of particle-free channel (filled circles) and micro-fluidized bed of 29.5 μm (empty circles), 34.5 μm (squares) and 39.5 μm glass (diamonds) micro-particles as a function of: (a) specific power dissipation; and (b) fluidized bed voidage. The arrows point to three points that are discussed in the text.

Conclusions

The mixing performance in a micro-fluidized bed with three different sized glass micro-particles (*i.e.* particle-to-channel size ratio) was examined experimentally using an optical method of dye dilution together with standard top-view imaging. Direct comparison with particle-free channel mixing was undertaken based on two efficiency parameters that account for the energy input: the mixing effectiveness of Kockmann *et al.* [26], and the energetic efficiency of mixing [51].

The micro-fluidized bed was found to afford mixing quality and, more importantly, efficiencies up to 3 time greater than those in the particle-free channel. The operating velocity and bed voidage influence significantly the performance of the micro-fluidized bed mixer. At the voidages close to that of a packed bed (*i.e.* low superficial fluid velocities), the micro-fluidized bed is not as effective as an empty channel. However, at voidages much beyond this it can offer enhancements in mixing.

The energetic efficiency of mixing for the micro-fluidized bed is a strong function of the specific power input, in line with other types of complex micro-mixers. However, an optimal specific power input is observed that corresponds to a voidage of around 0.78 for the smallest particle-to-channel size ratio considered here. Consideration of the variation of the mixing effectiveness factor of Kockmann *et al.* [26] with voidage suggests that the optimal voidage increases with particle-to-channel size ratio according to the simple empirical equation (n-1)/n, where n is Richardson-Zaki exponent.

In conclusion, micro-fluidized beds have potential in the microfluidics and process intensification context. However, the operating voidage is crucial in determining it's the energy efficiency performance.

Acknowledgement

The microchannel fabrication was performed at the South Australian node of the Australian National Fabrication Facility under the National Collaborative Research Infrastructure Strategy.

References

[1] V. Hessel, J.C. Schouten, A. Renken, J.-i. Yoshida, Micro process engineering: a comprehensive handbook, John Wiley & Sons, 2009.
[2] T. Wirth, Microreactors in organic chemistry and catalysis, 2nd ed., John Wiley & Sons, 2013.
[3] J.B. Marcinichen, J.A. Olivier, J.R. Thome, On-chip two-phase cooling of datacenters: Cooling system and energy recovery evaluation, Applied Thermal Engineering, 41 (2012) 36-51.
[4] T.G. Karayiannis, M.M. Mahmoud, Flow boiling in microchannels: Fundamentals and applications, Applied Thermal Engineering, in press.
[5] Q. Li, G. Flamant, X. Yuan, P. Neveu, L. Luo, Compact heat exchangers: A review and future applications for a new generation of high temperature solar receivers, Renewable and Sustainable Energy Reviews, 15 (2011) 4855-4875.
[6] J.E. Hesselgreaves, R. Law, D. Reay, Compact heat exchangers: selection, design and operation, Butterworth-Heinemann, 2016.
[7] X. Zhang, Y. Wang, P. Cang, R. Wang, Experimental investigation of thermal hydraulic performance of heat exchangers with different Reynolds numbers on both air-side and water-side, Applied Thermal Engineering, 99 (2016) 1331-1339.
[8] H.A. Stone, A.D. Stroock, A. Ajdari, Engineering Flows In Small Devices, Annual Review of Fluid Mechanics, 36 (2004) 381-411.
[9] T.M. Squires, S.R. Quake, Microfluidics: Fluid physics at the nanoliter scale, Reviews of Modern Physics, 77 (2005) 977.
[10] G.M. Whitesides, The origins and the future of microfluidics, Nature, 442 (2006) 368-373.
[11] K.E. Herold, A. Rasooly, Lab on a Chip Technology: Fabrication and microfluidics, Caister Academic Press, 2009.
[12] Á. Ríos, M. Zougagh, M. Avila, Miniaturization through lab-on-a-chip: Utopia or reality for routine laboratories? A review, Analytica Chimica Acta, 740 (2012) 1-11.
[13] J.P. Lafleur, A. Jönsson, S. Senkbeil, J.P. Kutter, Recent advances in lab-on-a-chip for biosensing applications, Biosensors and Bioelectronics, 76 (2016) 213-233.
[14] K.E. Herold, A. Rasooly, Lab on a Chip Technology: Fabrication and Microfluidics, Caister Academic Press, Norfolk, UK, 2009.
[15] C.D. Chin, V. Linder, S.K. Sia, Commercialization of microfluidic point-of-care diagnostic devices, Lab on a Chip, 12 (2012) 2118-2134.
[16] C.T. Culbertson, T.G. Mickleburgh, S.A. Stewart-James, K.A. Sellens, M. Pressnall, Micro Total Analysis Systems: Fundamental Advances and Biological Applications, Analytical Chemistry, 86 (2014) 95-118.

[17] M.L. Kovarik, P.C. Gach, D.M. Ornoff, Y. Wang, J. Balowski, L. Farrag, N.L. Allbritton, Micro Total Analysis Systems for Cell Biology and Biochemical Assays, Analytical Chemistry, 84 (2012) 516-540.
[18] L. Kang, B.G. Chung, R. Langer, A. Khademhosseini, Microfluidics for drug discovery and development: From target selection to product lifecycle management, Drug Discovery Today, 13 (2008) 1-13.
[19] F. Ahmad, S.A. Hashsham, Miniaturized nucleic acid amplification systems for rapid and point-of-care diagnostics: A review, Analytica Chimica Acta, 733 (2012) 1-15.
[20] J. Lee, S.A. Soper, K.K. Murray, Microfluidics with MALDI analysis for proteomics—A review, Analytica Chimica Acta, 649 (2009) 180-190.
[21] V. Hessel, H. Löwe, F. Schönfeld, Micromixers - a review on passive and active mixing principles, Chemical Engineering Science, 60 (2005) 2479-2501.
[22] N.-T. Nguyen, Micromixers: fundamentals, design and fabrication, William Andrew, 2011.
[23] L. Capretto, W. Cheng, M. Hill, X. Zhang, Micromixing Within Microfluidic Devices, in: B. Lin (ed.) Microfluidics, Vol. 304, Springer Berlin Heidelberg, 2011, pp. 27-68.
[24] V. Hessel, H. Löwe, F. Schönfeld, Micromixers—a review on passive and active mixing principles, Chemical Engineering Science, 60 (2005) 2479-2501.
[25] N.-T. Nguyen, Micromixers fundamentals, design, and fabrication, second edition, William Andrew, Waltham, Mass., 2012.
[26] N. Kockmann, T. Kiefer, M. Engler, P. Woias, Convective mixing and chemical reactions in microchannels with high flow rates, Sensors and Actuators B: Chemical, 117 (2006) 495-508.
[27] L. Falk, J.M. Commenge, Performance comparison of micromixers, Chemical Engineering Science, 65 (2010) 405-411.
[28] V. Zivkovic, M.J. Biggs, Z.T. Alwahabi, Experimental study of a liquid fluidization in a microfluidic channel, AIChE Journal, 59 (2013) 361-364.
[29] V. Zivkovic, M.J. Biggs, On importance of surface forces in a microfluidic fluidized bed, Chemical Engineering Science, 126 (2015) 143-149.
[30] J.J. Derksen, Scalar mixing with fixed and fluidized particles in micro-reactors, Chemical Engineering Research and Design, 87 (2009) 550-556.
[31] E. Doroodchi, M. Sathe, G. Evans, B. Moghtaderi, Liquid–liquid mixing using micro-fluidised beds, Chemical Engineering Research and Design, 91 (2013) 2235-2242.
[32] J.J. Derksen, Simulations of liquid-to-solid mass transfer in a fluidized microchannel, Microfluidics and Nanofluidics, (2014) 1-11.
[33] B. Potic, S.R.A. Kersten, M. Ye, M.A. van der Hoef, J.A.M. Kuipers, W.P.M. van Swaaij, Fluidization with hot compressed water in micro-reactors, Chemical Engineering Science, 60 (2005) 5982-5990.
[34] Z. Yang, M. Liu, C. Lin, Photocatalytic activity and scale-up effect in liquid–solid mini-fluidized bed reactor, Chemical Engineering Journal, 291 (2016) 254-268.
[35] I. Pereiro, A. Bendali, S. Tabnaoui, L. Alexandre, J. Srbova, Z. Bilkova, S. Deegan, L. Joshi, J.-L. Viovy, L. Malaquin, B. Dupuy, S. Descroix, A new microfluidic approach for the one-step capture, amplification and label-free quantification of bacteria from raw samples, Chemical Science, (2017) in press.
[36] E. Doroodchi, Z. Peng, M. Sathe, E. Abbasi-Shavazi, G.M. Evans, Fluidisation and packed bed behaviour in capillary tubes, Powder Technology, 223 (2012) 131-136.
[37] C. Tang, M. Liu, Y. Li, Experimental investigation of hydrodynamics of liquid–solid mini-fluidized beds, Particuology, 27 (2016) 102-109.
[38] O.L. do Nascimento, D.A. Reay, V. Zivkovic, Influence of surface forces and wall effects on the minimum fluidization velocity of liquid-solid micro-fluidized beds, Powder Technology, 304 (2016) 55-62.
[39] V. Zivkovic, M.N. Kashani, M.J. Biggs, Experimental and theoretical study of a micro-fluidized bed, AIP Conference Proceedings, 1542 (2013) 93-96.
[40] N. Epstein, Liquid-solids fluidization, in: W.-c. Yang (ed.) Handbook of fluidization and fluid-particle systems, CRC Press, New York, USA, 2003, pp. 705-764.
[41] G.M. Whitesides, E. Ostuni, S. Takayama, X. Jiang, D.E. Ingber, Soft lithography in biology and biochemistry, Annual Review of Biomedical Engineering, 3 (2001) 335-373.
[42] V. Zivkovic, P. Zerna, Z.T. Alwahabi, M.J. Biggs, A pressure drop correlation for low Reynolds number Newtonian flows through a rectangular orifice in a similarly shaped micro-channel, Chemical Engineering Research and Design, 91 (2013) 1-6.

[43] M. Navvab Kashani, V. Zivkovic, H. Elekaei, M.J. Biggs, A new method for reconstruction of the structure of micro-packed beds of spherical particles from desktop X-ray microtomography images. Part A. Initial structure generation and porosity determination, Chemical Engineering Science, 146 (2016) 337-345.
[44] M. Navvab Kashani, V. Zivkovic, H. Elekaei, L.F. Herrera, K. Affleck, M.J. Biggs, A new method for reconstruction of the structure of micro-packed beds of spherical particles from desktop X-ray microtomography images. Part B. Structure refinement and analysis, Chemical Engineering Science, 153 (2016) 434-443.
[45] J.F. Richardson, W.N. Zaki, The sedimentation of a suspension of uniform spheres under conditions of viscous flow, Chemical Engineering Science, 3 (1954) 65-73.
[46] M. Abramoff, P. Magalhaes, S.J. Ram, Image Processing with ImageJ, Biophotonics International, 11 (2004) 36-42.
[47] N.-T. Nguyen, Chapter 8 - Characterization techniques, in: Micromixers (Second Edition), William Andrew Publishing, Oxford, 2012, pp. 295-320.
[48] A. Hashmi, J. Xu, On the quantification of mixing in microfluidics, Journal of laboratory automation, 19 (2014) 488-491.
[49] H. Bruus, Theoretical Microfluidics, OUP Oxford, 2007.
[50] J.M. Ottino, W.E. Ranz, C.W. Macosko, A lamellar model for analysis of liquid-liquid mixing, Chemical Engineering Science, 34 (1979) 877-890.
[51] J. Baldyga, J.R. Bourne, Mixing and fast chemical reaction-VIII. Initial deformation of material elements in isotropic, homogeneous turbulence, Chemical Engineering Science, 39 (1984) 329-334.
[52] S. Ergun, Fluid flow through packed columns, Chemical Engineering Progress, 48 (1952) 89-94.
[53] S.-S. Hsieh, J.-W. Lin, J.-H. Chen, Mixing efficiency of Y-type micromixers with different angles, International Journal of Heat and Fluid Flow, 44 (2013) 130-139.
[54] M. Kashid, A. Renken, L. Kiwi-Minsker, Mixing efficiency and energy consumption for five generic microchannel designs, Chemical Engineering Journal, 167 (2011) 436-443.